

See discussions, stats, and author profiles for this publication at: <https://www.researchgate.net/publication/281143054>

High-Efficiency All-Dielectric Metasurfaces for Ultra-Compact Beam Manipulation in Transmission Mode

ARTICLE *in* NANO LETTERS · AUGUST 2015

Impact Factor: 13.59 · DOI: 10.1021/acs.nanolett.5b02926 · Source: PubMed

READS

172

6 AUTHORS, INCLUDING:



Mikhail I. Shalaev

University at Buffalo, The State University of N...

19 PUBLICATIONS 23 CITATIONS

[SEE PROFILE](#)



Jingbo Sun

University at Buffalo, The State University of N...

67 PUBLICATIONS 806 CITATIONS

[SEE PROFILE](#)



Apra Pandey

University at Buffalo, The State University of N...

12 PUBLICATIONS 21 CITATIONS

[SEE PROFILE](#)



Natalia Litchinitser

State University of New York

141 PUBLICATIONS 2,019 CITATIONS

[SEE PROFILE](#)

High-Efficiency All-Dielectric Metasurfaces for Ultracompact Beam Manipulation in Transmission Mode

Mikhail I. Shalaev,[†] Jingbo Sun,[†] Alexander Tsukernik,[‡] Apra Pandey,[§] Kirill Nikolskiy,^{||} and Natalia M. Litchinitser^{*,†}

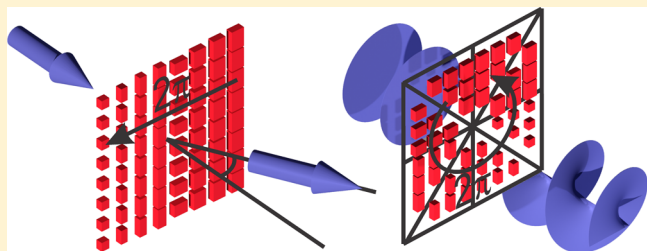
[†]Department of Electrical Engineering, University at Buffalo, The State University of New York, Buffalo, New York 14260, United States

[‡]Toronto Nanofabrication Centre, University of Toronto, Toronto, ON M5S 3G4, Canada

[§]CST, Inc., San Mateo, California 94404, United States

^{||}Physics Department, M.V. Lomonosov Moscow State University, Moscow 119991, Russia

ABSTRACT: Metasurfaces are two-dimensional structures enabling complete control on light amplitude, phase, and polarization. Unlike plasmonic metasurfaces, silicon structures facilitate high transmission, low losses, and compatibility with existing semiconductor technologies. We experimentally demonstrate two examples of high-efficiency polarization-sensitive dielectric metasurfaces with 2π phase control in transmission mode (45% transmission efficiency for the vortex converter and 36% transmission efficiency for the beam steering device) at telecommunication wavelengths. Silicon metasurfaces are poised to enable a versatile platform for the realization of all-optical circuitry on a chip.



KEYWORDS: All-dielectric metasurface, nanoblocks, singular optics, orbital angular momentum, structured light

Metasurfaces are two-dimensional artificial materials with thicknesses much smaller than incident light wavelength, allowing complete control of the phase, amplitude, and polarization of light beams.^{1–25} Compared to conventional optical elements, which rely on long propagation distances, these devices facilitate strong light-matter interaction on a subwavelength scale, allowing abrupt changes of beam parameters. Metasurfaces, unlike their three-dimensional analogues, metamaterials, do not require complicated fabrication techniques and can be produced in one lithographical step, which makes them very promising for integration on a photonic chip and well suited for mass production. To date, a majority of the studies has been focused on metal–dielectric structures, which have relatively low efficiency due to orthogonal polarizations coupling and nonradiative ohmic losses in metals.^{1,2,16} Many potential applications of metasurfaces, such as beam steering, lensing, holography, or structured light generation, would require full 2π phase control. However, it was shown that in the case of isolated single electric or magnetic resonance, only π phase shift is possible.^{1,2,26,27} While such phase manipulation can be obtained through cascading of multiple functional layers or by operating in reflection mode,^{1,2,25,28} metasurfaces realized using these approaches are not easily integratable on a chip and moreover, may not be compatible with contemporary semiconductor industry technologies or may not be well-suited for mass production.

Recently, it has been shown that high-refractive index nanoparticles embedded in a low-index surrounding medium

can be designed such that both magnetic and electric resonant responses occur in the same frequency range.^{29–35} It is the presence of both electric and magnetic resonances at the same frequencies allows a 2π phase control in a single-layer all-dielectric structure. It was shown that silicon nanostructures, having a relatively high refractive index at telecommunication wavelength, can be optimized to possess overlapping electric and magnetic dipole resonances in the same frequency range.^{26,27,36} There are several significant advantages of using dielectric nanoparticles as compared to metallic nanostructures such as, for example, V-shaped antennas.^{37,38} In particular, dielectric nanostructures enable high transmission efficiency because they do not suffer from intrinsic nonradiative losses in metals. Moreover, no orthogonal polarizations coupling, cascading, or working in reflection mode is required to achieve full 2π phase control. Also, silicon is the most commonly used material in the semiconductor industry, which makes it an ideal platform for high-efficiency metasurfaces for near-infrared (NIR) wavelength and future integration on optical chip.

First, we consider light propagation through an infinite array of high refractive index polysilicon nanoblocks (refractive index $n = 3.67$ with height $h = 270$ nm and dimensions $dx = dy = 650$ nm on top of semi-infinite fused silica substrate (refractive index $n_s = 1.45$, lattice constant $a = 800$ nm (Figure 1a). We

Received: July 24, 2015

Revised: August 14, 2015

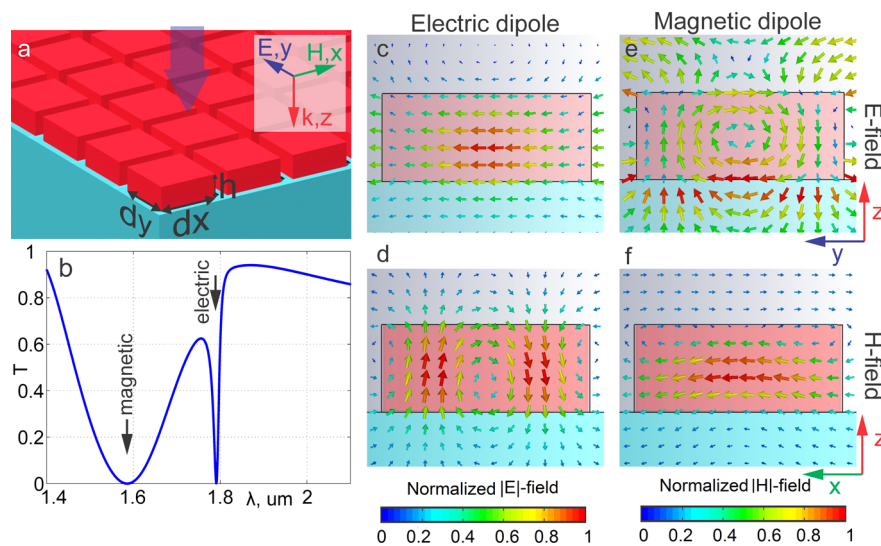


Figure 1. (a) Schematics of an infinite array of silicon nanoblocks metasurface on top of bulk-fused silica substrate. Nanoblocks height $h = 270$ nm, dimensions along x and y axes $dx = dy = 650$ nm, lattice constant $a = 800$ nm. (b) Transmittance spectrum of metasurfaces shows two dips for magnetic ($\lambda_m = 1.6 \mu\text{m}$) and electric ($\lambda_e = 1.8 \mu\text{m}$) resonances. (c,d) Electric field enhancement at the center of silicon nanoblocks and vortex-like magnetic field distribution indicates electric resonance, while the opposite holds for magnetic resonance (e,f) with H-field maximum at the center and twisted E-field around it. Electric and magnetic fields amplitudes are normalized to their maximum values in each image.

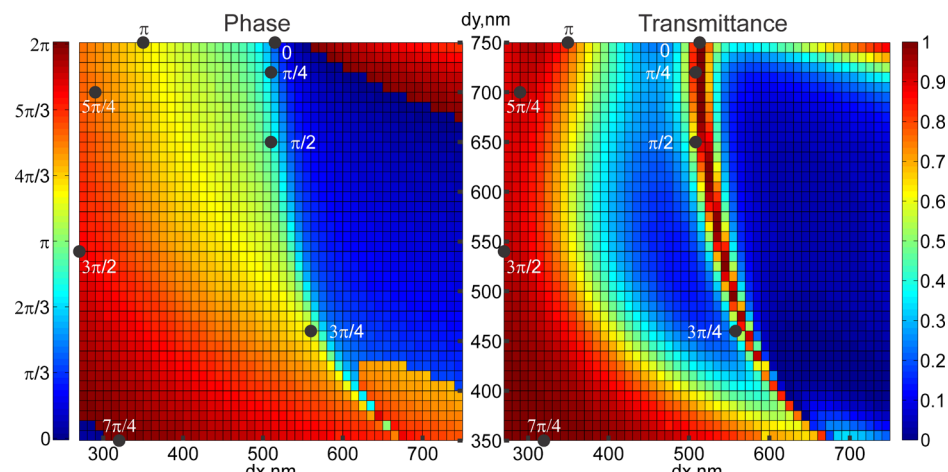


Figure 2. (a) Transmitted light phase variation for nanoblocks on silicon dioxide substrate with lattice constant and (b) transmittance as a function of silicon block size dx and dy .

Table 1. Optimized Nanoblocks Dimensions

phase	0	$\pi/4$	$\pi/2$	$3\pi/4$	π	$5\pi/4$	$3\pi/2$	$7\pi/4$
dx , nm	515	510	510	560	350	290	270	320
dy , nm	750	720	650	460	750	700	540	350
T , %	94	83	94	85	79	92	93	99

used commercially available CST MICROWAVE STUDIO software to perform numerical simulation; the incident electromagnetic field was assumed to be a plane wave, propagating along z -axis with electric and magnetic fields polarized along y - and x -axes, correspondingly. The transmission spectrum, shown in Figure 1b, clearly shows two dips corresponding to resonant interaction with metasurfaces and as a result near unity reflection, while the structure was assumed to be lossless. Electric and magnetic field distributions in the unit cell cross-section show electric resonance behavior for wavelength around $\lambda_e = 1.8 \mu\text{m}$, with E-field concentrated at the center of nanoblocks and vortex-like H-field distribution

around electric field (Figure 1c,d). The opposite holds for magnetic resonance around $\lambda_m = 1.6 \mu\text{m}$ with magnetic field maximum at the center in the $y-z$ plane and vortex-like electric field around in the $x-z$ plane (Figure 1e,f). Electric and magnetic fields amplitudes are normalized to its maximum in each image. In this example, electric and magnetic resonances are well-separated and can be easily distinguished. However, as the block size decreases the spacing between the resonances decreases such that two resonances shift toward the wavelength of interest. Once the resonances overlap, enabling the impedance matching, nearly 100% transmission with full 2π phase control can be achieved.^{29,39,40} We calculate transmitted beam phase as a function of silicon block size along x - and y -axes. Note that the possibility of varying the dimensions of the nanoblocks in both x - and y -directions adds additional degrees of freedom and allows the design of polarization-dependent metasurfaces; polarization-independent design is also possible and was studied in refs 27, 34, and 35. In this work, the wavelength of interest $\lambda_0 = 1.55 \mu\text{m}$, lattice constant $a = 800$

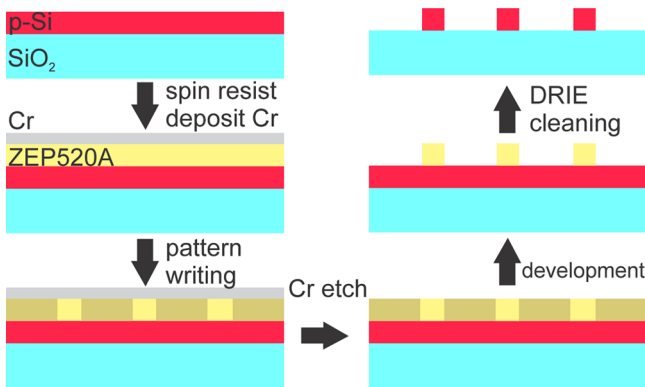


Figure 3. Fabrication process for silicon-based dielectric metasurfaces. Polycrystalline silicon was deposited on top of fused silica wafers by LPCVD, followed by spin coating of e-beam resist ZEP520A and deposition of 20 nm charge dissipation Cr layer. Then pattern was written by EBL and Cr layer was etched by ceric ammonium nitrate-based etchant. Samples were developed in ZED-N50 followed by DRIE, removal of resist and O₂ plasma cleaning.

nm, and silicon nanoblock height $h = 270$ nm. **Figure 2** shows the results of numerical simulation for phase and corresponding transmittance as a function of dx and dy . As one of the advantages of the all-dielectric metasurface design is the possibility of high transmission through the structure, we use the results of these numerical simulations to simultaneously enable 0 to 2π variation of the phase as well as transmission around 90%. Also, we limit the dimensions of the nanoblocks to be less than 750 nm. This requirement is due to fabrication constraints as we fixed the lattice constant to be 800 nm. The results shown in **Figure 2** are general rather than application specific, and therefore they can be used to design a number of functionalities.

We choose eight discrete nanoblocks with $\pi/4$ increments to cover 0-to- 2π phase to provide full phase control of the

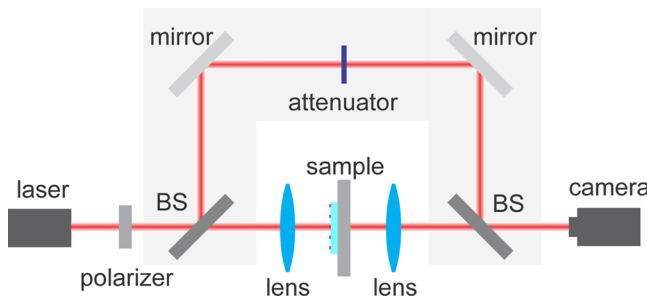


Figure 5. Schematics of experimental setup for measurement of fabricated metasurfaces. Diode NIR laser was used as a light source followed by light polarizer, beam was focused to the sample by lens, then collimated and image was captured with camera. Setup for vortex beam interference is shown in gray background; it contains attenuator, two beam splitters, and mirrors.

wavefront. **Table 1** shows transmitted light phase and transmittance depending on nanoblocks dimensions.

For experimental verification of our numerical simulations, we deposited 270 nm of silicon with low-pressure physical vapor deposition (LPCVD) on top of fused quartz wafers. Fabrication process is shown in **Figure 3**. The refractive index of deposited silicon was measured to be $n = 3.67$ at 1.55 μm using spectroscopic ellipsometry. We used standard electron-beam lithography (EBL) with ZEP520A resist; due to the strong charging effect of nonconductive SiO₂ substrate, 20 nm thick charge dissipation Cr layer was deposited on the e-beam resist. The EBL pattern writing was followed by Cr etching with commercially available Cr etchant and development in ZED-N50. Then deep reactive ion etching (DRIE) was performed in C₄F₈ and SF₆ gases, followed by resist removing in Remover 1165 at 80 °C for 1 h and 5 min O₂ plasma for removal of resist residue.

We experimentally demonstrated high-efficiency full-phase manipulation with dielectric metasurfaces at near-infrared wavelength enabling two practical functionalities: optical

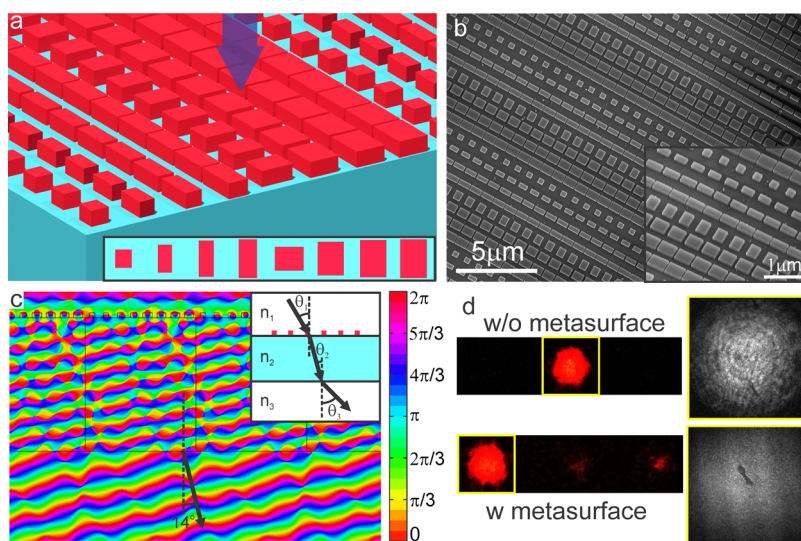


Figure 4. (a) Schematics of the proposed beam deflector with the unit cell (shown in the inset) containing eight nanoblocks, each responsible for the phase shift from 0 to 2π with $\pi/4$ increments. (b) Scanning electron microscopy image of fabricated metasurfaces with 96 × 96 μm total size; zoomed-in picture is shown in the inset. (c) Numerically simulated phase of plane wave propagating through the metasurfaces on SiO₂ substrate showing refracted beam angle around 14°. (d) Beam position without (left top) and with (left bottom) metasurface; the beam power is refracted to the left side with deflection angle 13.1° and transmission of ~36%. Input and output beam photographs are also shown in the inset (right).

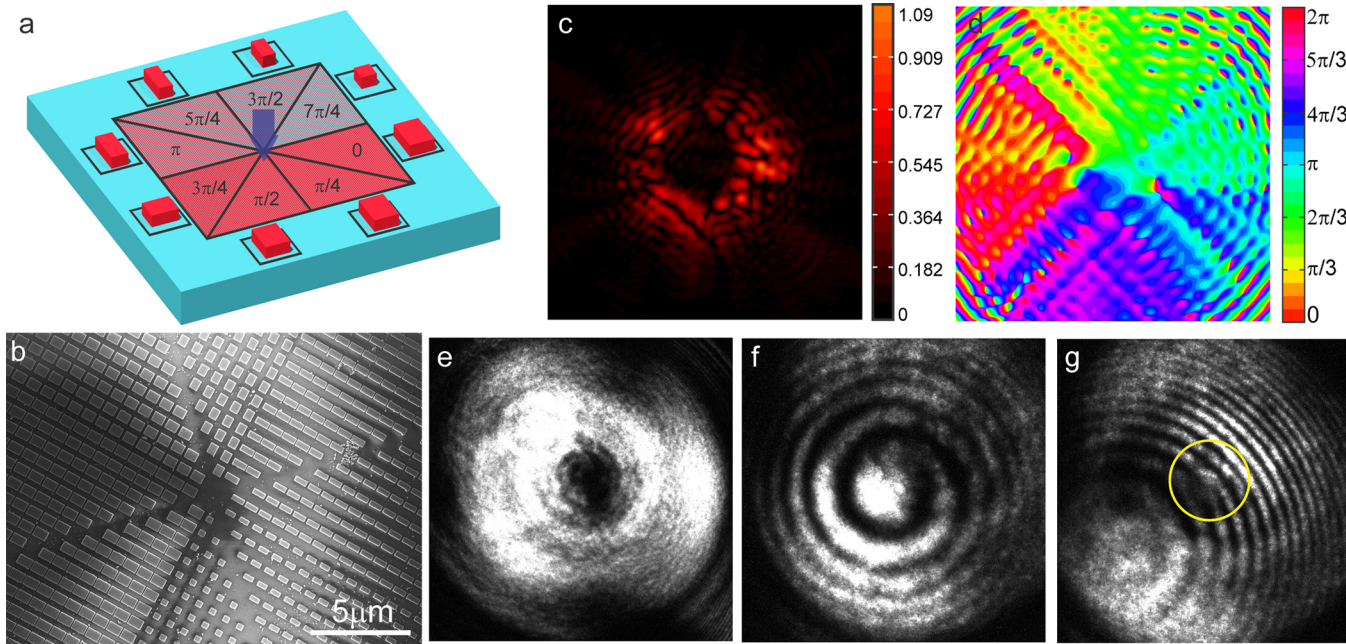


Figure 6. (a) Schematics and (b) scanning electron microscopy image for optical vortex beam converter with eight sectors with nanoblocks from Table 1, unit cells for each sector of metasurface are shown. Each sector introduce an additional $\pi/4$ phase shift, thus covering 0 to 2π phase change. (c,d) Numerically calculated normalized amplitude and phase distribution. (e) Intensity distribution for measured output vortex beam in form of donut shape. (f,g) Vortex and Gaussian beams interference experiment results showing spiral-shaped and fork-like intensity distribution.

beam steering and conversion of a conventional Gaussian beam into a beam with an orbital angular momentum (OAM) or a vortex beam. In both cases, dramatic changes on light propagation take place within a distance of less than $\lambda/5$, opening new possibilities of light control with semiconductor-industry-compatible materials and an easy fabrication procedure.

Figure 4a,b shows schematics and scanning electron microscopy (SEM) images for a fabricated beam deflecting metasurface with $96 \times 96 \mu\text{m}$ total size, unit cell is shown in inset. The metasurface contains eight nanoblocks from Table 1, where each is responsible for a phase shift from 0 to 2π with $\pi/4$ increments. We consider light propagation from isotropic medium 1 to the medium 3 through bulk substrate with the metasurface on top as shown in the inset in Figure 4c. Deflection angle for a beam can be calculated with the following equation³⁸ $\theta_3 = \sin^{-1}[(n_1 \sin \theta_1 + \lambda_0/\Gamma)/n_3]$, where n_1 and n_3 are refractive indices for media 1 and 3, θ_1 is the incidence angle, λ_0 is the free-space wavelength of light, and Γ is the periodicity of the structure. We consider normal incidence of a light beam on the metasurface with the period of the structure $\Gamma = 6.4 \mu\text{m}$ fabricated on the substrate surrounded by air. In this case, the angle of refraction is $\theta_3 \approx 14^\circ$. We consider plane wave light propagation through infinite two-dimensional periodic array of silicon nanoblocks. Numerical simulations confirm the theoretically calculated refraction angle, as shown in Figure 4c.

We used a diode laser as a light source to perform measurements for beam steering using a NIR detector card to determine deflected beam position; schematic of experimental setup is shown in Figure 5. The card converts invisible IR signal to visible region; thus, deflected beam position was captured by visible light camera. The laser beam was focused by lens to the spot with approximately $45 \mu\text{m}$ waist. Inset on the left in Figure 4d shows the results of beam-position

measurement without (top) and with (bottom) metasurface. As can be seen, the beam power is refracted to the left side of the screen, while other diffraction orders can be also seen. The presence of other diffraction orders with much smaller intensities compared to the main beam can be caused by the fact that the unit cell size is comparable to wavelength of light,⁴¹ by imperfections in fabrication process and violation of local periodicity assumed in our design. The refraction angle for the main beam is measured to be 13.1° , which is close to theoretical and numerical simulations' predictions. Insets on the right show NIR camera images of input and output beams with measured transmission power to desired order normalized on input power to be around 36%.

Finally, to demonstrate flexibility of designed dielectric nanoblocks for phase control, we fabricated a spatial light modulator that converts a regular Gaussian laser beam into an OAM beam, or vortex. Such structured light beams have a potential for applications ranging from quantum information processing and high-dimensional communication systems to optical manipulation on nanoscale.^{11,23,24,42,43} Schematics of fabricated metasurface for twisted beam generation is shown in Figure 6a, which contains eight sectors for the particular 0-to- 2π phase shift. Optical vortices, unlike conventional Gaussian beams, possess a donut-shape intensity profile and helical wavefront with phase change from 0 to 2π in cross-section. Fabricated beam converter SEM image is shown in Figure 6b, where the total size of the sample is $96 \times 96 \mu\text{m}$. We performed numerical simulations in CST MICROWAVE STUDIO software package for reduced size model with $67.2 \times 67.2 \mu\text{m}$ size to reduce calculation time and memory consumption. Figure 6c,d shows the results of numerical simulations corresponding to the normalized transmitted beam intensity and phase at distance of $0.5\lambda_0$ from metasurface, respectively. Transmittance for numerically simulated light propagation is 56.4%. Corresponding experimentally measured intensity

profile is shown in Figure 6e. In order to prove the presence of the helical wavefront, we also performed the interference experiments for both cases of parallel and tilted Gaussian beam interfering with the beam obtained from the metasurface. Resulting spiral- and fork-like intensity profiles are shown in Figure 6f,g, respectively. Transmitted power normalized to input power was measured to be 45% which is close to numerically simulated value.

In summary, we have experimentally demonstrated an all-dielectric resonant metasurface with full 0-to- 2π phase control at NIR wavelength. We designed and fabricated high-efficiency beam deflector and light converter for generating optical vortex beam, carrying an OAM. In addition to 0 to π phase control enabled by a single magnetic or electric resonance, overlapping of magnetic and electric resonances in the frequency domain enable an additional phase control with optical impedance matching and, as a result, high efficiency in transmission mode with full 2π phase manipulation. In sharp contrast to plasmonic metasurfaces, fabricated devices made with silicon are compatible with complementary metal–oxide–semiconductor technology. Demonstrated metasurfaces have relatively high transmission coefficients of 36% for beam deflector and 45% for vortex beam converter. These devices can be fabricated in one lithographical step, alleviating the need for cascading or working in reflection mode to achieve full phase control. Silicon-based metasurfaces can be used for fabrication of miniaturized high-efficiency optical components for NIR photonics, such as flat lenses, beam deflectors, antireflection coatings, and phase modulators. Elimination of metals and, as a result, no ohmic losses, compared to plasmonic counterparts and not requiring cross-polarized field interaction to cover full phase, makes them well-suited for integration on optical chip and for large-scale production.

AUTHOR INFORMATION

Corresponding Author

*E-mail: natalash@buffalo.edu.

Author Contributions

The manuscript was prepared in a collaborative effort of all authors. All authors have given approval to the final version of the manuscript. N.M.L. and M.I.S. proposed the idea developed in this work. M.I.S., J.S., A.P., and K.N. made the design and performed the numerical simulations. M.I.S. and A.T. did the fabrication of the samples. J.S. and M.I.S. performed the optical characterization of the sample. N.M.L. and M.I.S. wrote the paper. N.M.L. supervised this work.

Notes

The authors declare no competing financial interest.

ACKNOWLEDGMENTS

This work was supported by the U.S. Army Research Office Award No. W911NF-11-1-0333. The authors would like to thank Professor Gennady Shvets and his research group at the University of Texas at Austin for very useful comments on the manuscript.

REFERENCES

- (1) Zhao, Y.; Liu, X. X.; Alu, A. *J. Opt.* **2014**, *16*, 123001.
- (2) Yu, N.; Capasso, F. *Nat. Mater.* **2014**, *13*, 139–150.
- (3) Lin, D. M.; Fan, P. Y.; Hasman, E.; Brongersma, M. L. *Science* **2014**, *345*, 298–302.
- (4) Kim, S. W.; Yee, K. J.; Abashin, M.; Pang, L.; Fainman, Y. *Opt. Lett.* **2015**, *40*, 2453–2456.

- (5) Minovich, A. E.; Miroshnichenko, A. E.; Bykov, A. Y.; Murzina, T. V.; Neshev, D. N.; Kivshar, Y. S. *Laser Photon. Rev.* **2015**, *9*, 195–213.
- (6) Wu, C. H.; Arju, N.; Kelp, G.; Fan, J. A.; Dominguez, J.; Gonzales, E.; Tutuc, E.; Brener, I.; Shvets, G. *Nat. Commun.* **2014**, *5*, 3892.
- (7) Ni, X. J.; Kildishev, A. V.; Shalaev, V. M. *Nat. Commun.* **2013**, *4*, 2807.
- (8) West, P. R.; Stewart, J. L.; Kildishev, A. V.; Shalaev, V. M.; Shkunov, V. V.; Strokhendl, F.; Zakharenkov, Y. A.; Dodds, R. K.; Byren, R. *Opt. Express* **2014**, *22*, 26212–26221.
- (9) Farmahini-Farahani, M.; Cheng, J. R.; Mosallaei, H. *J. Opt. Soc. Am. B* **2013**, *30*, 2365–2370.
- (10) Buchnev, O.; Podoliak, N.; Kaczmarek, M.; Zheludev, N. I.; Fedotov, V. A. *Adv. Opt. Mater.* **2015**, *3*, 674–679.
- (11) Li, G. X.; Kang, M.; Chen, S. M.; Zhang, S.; Pun, E. Y. B.; Cheah, K. W.; Li, J. S. *Nano Lett.* **2013**, *13*, 4148–4151.
- (12) Sun, S. L.; Yang, K. Y.; Wang, C. M.; Juan, T. K.; Chen, W. T.; Liao, C. Y.; He, Q.; Xiao, S. Y.; Kung, W. T.; Guo, G. Y.; Zhou, L.; Tsai, D. P. *Nano Lett.* **2012**, *12*, 6223–6229.
- (13) Sautter, J.; Staude, I.; Decker, M.; Rusak, E.; Neshev, D. N.; Brener, I.; Kivshar, Y. S. *ACS Nano* **2015**, *9*, 4308–4315.
- (14) Bohn, B. J.; Schnell, M.; Kats, M. A.; Aieta, F.; Hillenbrand, R.; Capasso, F. *Nano Lett.* **2015**, *15*, 3851–3858.
- (15) Genevet, P.; Capasso, F. *Rep. Prog. Phys.* **2015**, *78*, 024401.
- (16) Kildishev, A. V.; Boltasseva, A.; Shalaev, V. M. *Science* **2013**, *339*, 1232009.
- (17) Bomzon, Z.; Biener, G.; Kleiner, V.; Hasman, E. *Opt. Lett.* **2002**, *27*, 1141–1143.
- (18) Pfeiffer, C.; Emani, N. K.; Shaltout, A. M.; Boltasseva, A.; Shalaev, V. M.; Grbic, A. *Nano Lett.* **2014**, *14*, 2491–2497.
- (19) Holloway, C. L.; Kuester, E. F.; Gordon, J. A.; O'Hara, J.; Booth, J.; Smith, D. R. *IEEE Antennas Propag. Mag.* **2012**, *54*, 10–35.
- (20) Bomzon, Z.; Kleiner, V.; Hasman, E. *Appl. Phys. Lett.* **2001**, *79*, 1587–1589.
- (21) Bomzon, Z.; Kleiner, V.; Hasman, E. *Opt. Lett.* **2001**, *26*, 1424–1426.
- (22) Yin, X. B.; Ye, Z. L.; Rho, J.; Wang, Y.; Zhang, X. *Science* **2013**, *339*, 1405–1407.
- (23) Karimi, E.; Schulz, S. A.; De Leon, I.; Qassim, H.; Upham, J.; Boyd, R. W. *Light: Sci. Appl.* **2014**, *3*, e167.
- (24) Bouchard, F.; De Leon, I.; Schulz, S. A.; Upham, J.; Karimi, E.; Boyd, R. W. *Appl. Phys. Lett.* **2014**, *105*, 101905.
- (25) Yi, X. N.; Ling, X. H.; Zhang, Z. Y.; Li, Y.; Zhou, X. X.; Liu, Y. C.; Chen, S. Z.; Luo, H. L.; Wen, S. C. *Opt. Express* **2014**, *22*, 17207–17215.
- (26) Staude, I.; Miroshnichenko, A. E.; Decker, M.; Fofang, N. T.; Liu, S.; Gonzales, E.; Dominguez, J.; Luk, T. S.; Neshev, D. N.; Brener, I.; Kivshar, Y. S. *ACS Nano* **2013**, *7*, 7824–7832.
- (27) Cheng, J. R.; Ansari-Oghol-Beig, D.; Mosallaei, H. *Opt. Lett.* **2014**, *39*, 6285–6288.
- (28) Yang, Y. M.; Wang, W. Y.; Moitra, P.; Kravchenko, II; Briggs, D. P.; Valentine, J. *Nano Lett.* **2014**, *14*, 1394–1399.
- (29) Fu, Y. H.; Kuznetsov, A. I.; Miroshnichenko, A. E.; Yu, Y. F.; Luk'yanchuk, B. *Nat. Commun.* **2013**, *4*, 1527.
- (30) Person, S.; Jain, M.; Lapin, Z.; Saenz, J. J.; Wicks, G.; Novotny, L. *Nano Lett.* **2013**, *13*, 1806–1809.
- (31) Geffrin, J. M.; Garcia-Camara, B.; Gomez-Medina, R.; Albella, P.; Froufe-Perez, L. S.; Eyrraud, C.; Litman, A.; Vaillon, R.; Gonzalez, F.; Nieto-Vesperinas, M.; Saenz, J. J.; Moreno, F. *Nat. Commun.* **2012**, *3*, 1171.
- (32) Pfeiffer, C.; Grbic, A. *Phys. Rev. Lett.* **2013**, *110*, 197401.
- (33) Neuner, B., III; Wu, C.; Ten Eyck, G.; Sinclair, M.; Brener, I.; Shvets, G. *Appl. Phys. Lett.* **2013**, *102*, 211111.
- (34) Yu, Y. F.; Zhu, A. Y.; Paniagua-Dominguez, R.; Fu, Y. H.; Luk'yanchuk, B.; Kuznetsov, A. I. *Laser Photonics Rev.* **2015**, *9*, 412–418.
- (35) Chong, K. E.; Staude, I.; James, A.; Dominguez, J.; Liu, S.; Campione, S.; Subramania, G. S.; Luk, T. S.; Decker, M.; Neshev, D. N.; Brener, I.; Kivshar, Y. S. *Nano Lett.* **2015**, *15*, 5369–5374.

- (36) Decker, M.; Staude, I.; Falkner, M.; Dominguez, J.; Neshev, D. N.; Brener, I.; Pertsch, T.; Kivshar, Y. S. *Adv. Opt. Mater.* **2015**, *3*, 813–820.
- (37) Papakostas, A.; Potts, A.; Bagnall, D. M.; Prosvirnin, S. L.; Coles, H. J.; Zheludev, N. I. *Phys. Rev. Lett.* **2003**, *90*, 107404.
- (38) Yu, N. F.; Genevet, P.; Kats, M. A.; Aieta, F.; Tetienne, J. P.; Capasso, F.; Gaburro, Z. *Science* **2011**, *334*, 333–337.
- (39) Van de Groep, J.; Polman, A. *Opt. Express* **2013**, *21*, 26285–26302.
- (40) Evlyukhin, A. B.; Eriksen, R. L.; Cheng, W.; Beermann, J.; Reinhardt, C.; Petrov, A.; Prorok, S.; Eich, M.; Chichkov, B. N.; Bozhevolnyi, S. I. *Sci. Rep.* **2014**, *4*, 4126.
- (41) Larouche, S.; Smith, D. R. *Opt. Lett.* **2012**, *37*, 2391–2393.
- (42) Wang, J.; Yang, J. Y.; Fazal, I. M.; Ahmed, N.; Yan, Y.; Huang, H.; Ren, Y. X.; Yue, Y.; Dolinar, S.; Tur, M.; Willner, A. E. *Nat. Photonics* **2012**, *6*, 488–496.
- (43) Willner, A. E.; Wang, J.; Huang, H. *Science* **2012**, *337*, 655–656.